

# Enhancement of the evanescent field using polymer waveguides fabricated by deep UV exposure on mesoporous silicon

Dominik G. Rabus,<sup>1,\*</sup> Lisa A. DeLouise,<sup>2</sup> and Yasuhisa Ichihashi<sup>3</sup>

<sup>1</sup>University of California, Santa Cruz, Baskin School of Engineering, 1156 High Street, Santa Cruz, California 95064, USA

<sup>2</sup>University of Rochester Medical Center, 601 Elmwood Avenue, Dermatology 6-6823, Rochester, New York 14642, USA

<sup>3</sup>Forschungszentrum Karlsruhe, Institute for Microstructure Technology, P.O. Box 3640, 76021 Karlsruhe, Germany

\*Corresponding author: rabus@soe.ucsc.edu

Received June 27, 2007; revised August 24, 2007; accepted August 26, 2007;  
posted August 29, 2007 (Doc. ID 84610); published September 26, 2007

Polymer integrated reverse symmetry waveguides on porous silicon substrate fabricated by using deep ultraviolet radiation in poly(methyl methacrylate) are presented. The layer sequence and geometry of the waveguide enable an evanescent field extending more than 3  $\mu\text{m}$  into the upper waveguide or analyte layer, enabling various integrated optical devices where large evanescent fields are required. The presented fabrication technique enables the generation of defined regions where the evanescent field is larger than in the rest of the waveguide. This technology can improve the performance of evanescent-wave-based waveguide devices. © 2007 Optical Society of America  
OCIS codes: 130.5460, 130.3130.

Considerable interest has been focused on optical devices that are based on the interactions associated with evanescent waves, such as directional couplers and waveguide sensors. These devices make use of the electromagnetic field that propagates in the waveguide, creating an evanescent field that extends into the surrounding layers present at the surface of the waveguide. For example, commercial success has been realized by employing surface plasmon resonance spectroscopy for optical biosensing of substances extending  $\sim 200$  nm from the transducer surface. Several techniques have been presented in order to enhance the evanescent field to improve the performance of the devices, particularly for optical studies of cells. Nesnidal and Walker use a multilayer dielectric structure to enhance the evanescent waves [1]. Quigley *et al.* use thin high-index films for evanescent field enhancement [2]. A novel use of metamaterials is presented in [3] for increasing the evanescent field. Recently a so-called planar reverse symmetry waveguide has been demonstrated [4,5], where the substrate has a refractive index less than the refractive index of the cladding layer, enabling the extension of the evanescent field ( $>1$   $\mu\text{m}$ ) into the analyte present on the surface of the waveguide. In this Letter we report a novel fabrication process utilizing standard wafer fabrication processing for realizing what is to our knowledge the first integrated reverse symmetry (IRS) waveguide.

A conventional integrated waveguide is made up of a substrate, a waveguiding layer, and a so-called cladding layer that covers the waveguiding layer. In this configuration, the waveguide's index of refraction is usually higher than the cladding layer. The exponentially decaying evanescent field in this configuration typically penetrates into the cladding layer 100–300 nm, which is sufficient for many integrated optical devices but not enough for devices requiring

large evanescent fields. IRS waveguides solve this problem by choosing a lower cladding layer having a lower refractive index than the upper cladding layer, in our case electrochemically formed mesoporous silicon (PSi) [6]. The PSi layer not only enables a lower cladding having a lower refractive index, but also optically isolates the waveguide core from the Si substrate. As Si has a refractive index ( $\sim 3.5$ ) much higher than that of typical polymers ( $\sim 1.5$ – $1.7$ ), a thick lower cladding layer must be used to avoid light coupling with the substrate. Oliveri *et al.* [7] have found that a 3  $\mu\text{m}$  thick porous silica layer as a lower cladding is sufficient to fabricate polymer waveguides on a Si wafer.

The fabrication of the IRS waveguide described here is based on the deep ultraviolet (DUV) modification of a polymer [8] [in our case poly(methyl methacrylate) (PMMA)] coated on top of PSi for realizing the waveguiding layer. The DUV technique enables the realization of single-mode waveguides [9] that are able to cover a wide wavelength range ( $\sim 300$  to  $\sim 1700$  nm) [10]. A few-micrometer thin waveguide layer with higher refractive index (difference between the unexposed and exposed polymer,  $\Delta n = 0.008$ – $0.015$ ) can be formed in a thicker PMMA layer with a lower refractive index. By designing the thickness and the width of the high-index PMMA layer, it is possible to realize single-mode DUV waveguides for the transparency region of PMMA. The layer sequence and the dimensions of our IRS waveguide are shown in Fig. 1a.

IRS waveguide fabrication begins with electrochemical formation of a PSi substrate layer in a p+ Si wafer (0.01 ohm cm) by using an electrolyte consisting of 30 ml hydrofluoric acid (48%) and 70 ml ethanol (95%). The barrier layer is a thin ( $<12$  nm), low-porosity layer (60%) etched by using a current density of 5 mA/cm<sup>2</sup>, which produces a pore struc-

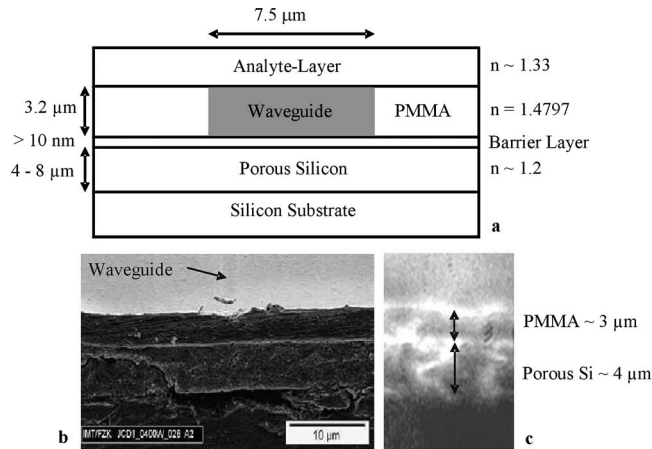


Fig. 1. IRS waveguide. a, Layer sequence and layout. b, Scanning electron microscope image of reverse symmetry waveguide. c, Near-field image of outcoupling waveguide facet.

ture with diameters less than  $\sim 5$  nm (Fig. 2a). This is followed by a thick 4–8  $\mu\text{m}$  high-porosity (80%–90%) optical isolation layer etched by using a current density of 50–70  $\text{mA}/\text{cm}^2$ , which produces more open pore diameters ranging between 20 and 30 nm (Fig. 2b). The PMMA layer (Resist MicroChem 950k PMMA A11) is spin coated (Spincoater Hamatech, 2000/15/2 [rpm/ramp/min]) onto the PSi substrate to a thickness of approximately 3  $\mu\text{m}$ . The sample is annealed at 170°C for 30 min. A DUV lithography system (EVG620) is used for fabricating the waveguides under vacuum with a quartz/chromium mask. The illumination dose used is 3  $\text{J}/\text{cm}^2$ . The samples are then annealed at 70°C for 4 h. The final step is the dicing of the samples to provide waveguide end faces for optical measurements.

Direct spin-coating of polymers is usually not feasible when using porous substrates, as the solvent and polymer can infiltrate the pores, which will raise the refractive index. To prevent this Horvath *et al.* [11] used a technique referred to as dip floating,

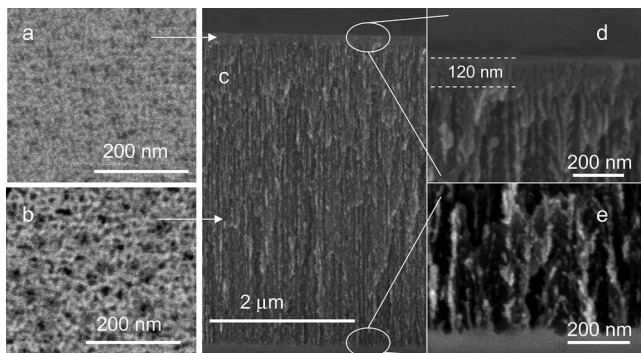


Fig. 2. SEM images of mesoporous bilayer structure. a, Pore structure of barrier layer (5  $\text{mA}/\text{cm}^2$ ). b, Pore structure of optical isolation layer (50  $\text{mA}/\text{cm}^2$ ). c, Side view of bilayer structure, illustrating anisotropic growth of pore channels and porosity contrast between barrier and optical isolation layers. d, Magnified view of barrier layer grown intentionally thick (120 nm) to observe with a scanning electron microscope. e, Magnified view of porous tip-Si wafer interface.

which requires several fabrication steps. Our process prevents polymer resist from infiltrating too deep into the optical isolation layer by monolithic integration of the PSi bilayer structure, described above, comprised of a low-porosity barrier layer on top of the high-porosity optical isolation layer (Fig. 2). Bilayer formation leverages the ability to tune PSi morphology simply by altering current density during the electrochemical etch process. Our studies find that the PSi barrier layer is crucial for enabling waveguide performance. We have fabricated several porous Si configurations with and without the barrier layer. The fabrication parameters for the samples tested are summarized in Table 1. The refractive index of the optical isolation layer is estimated by using the Bruggman effective medium approximation [12].

The IRS waveguides are characterized by using an optical fiber mounted onto a piezo electrically driven XYZ stage for coupling into the waveguides. A microscope objective (100 $\times$ ) is used on the outcoupling side and focuses the near-field image onto an IR camera (Hamamatsu Model C2400). All measurements are carried out at a wavelength of 1550 nm. Shifting to other wavelengths is, however, possible, as only the design (width and DUV exposure dose) of the integrated reverse symmetry waveguides has to be adjusted to guarantee single-mode operation at the required wavelength. A near-field image of the facet of sample 3 is shown in Fig. 1c without light from the laser source being coupled into the waveguide. The results from the near-field measurements on samples 2, 3, 4 and 5 are presented in Fig. 3.

To demonstrate IRS waveguide performance, measurements are performed by taking the near-field image of samples with and without water on top of the waveguides to determine the expansion of the mode traveling in the waveguide. We have chosen water to be the cladding layer, as its refractive index ( $n = 1.333$ ) is sufficient to demonstrate the performance and it is relevant to our future goals of utilizing this device for aqueous-based biosensing applications. Replacing the water by a suitable polymer having the appropriate refractive index would be of course state of the art. The water is placed directly on top of the waveguides, and it is made sure that the water is also at the outcoupling facet, making it possible to see the portion of the mode penetrating into the water.

Results find that only the integrated reverse symmetry waveguides with the low-porosity PSi barrier layer showed the desired evanescent field enhancement of a deep penetration of the evanescent field into the upper analyte layer. The height of the mode field nearly doubles as can be seen in the near-field images of samples 2 and 5 in Fig. 3 with the analyte layer present. Because the mode is confined in the polymer layer, which is  $\sim 3$   $\mu\text{m}$  in the absence of the analyte layer, the height of the evanescent field in the presence of the analyte layer can be approximated to be more than 3  $\mu\text{m}$ . The evanescent field decays into the water even when the refractive index is estimated to be 1.38, which is slightly higher than that of water. The measurements also confirm that in the

**Table 1. Fabrication Parameters of Porous Si Layers**

Sample	Layers	Etch Conditions Current Density (mA/cm <sup>2</sup> )/s	Porosity (%)	Thickness ( $\mu\text{m}$ )	Refractive Index
2	2	5/1, 50/138	60, 77	0.010, 4	1.83, 1.38
3	1	70/108	84	4	1.21
4	1	70/216	84	8	1.21
5	2	5/1, 70/216	60, 84	0.010, 8	1.83, 1.21

absence of the barrier layer, the spin coated polymer fills up the pores, as is visible, for example, in the near-field image of sample 3 in Fig. 3, leading to an unwanted conventional waveguide having an evanescent field that decays only a few 100 nm into the upper analyte layer.

Efforts to characterize waveguide loss using the cutback method proved difficult to determine the losses accurately, as our samples are only 1 cm  $\times$  1 cm and dicing introduced more losses at the in-

terface, as can be seen in Fig. 1b. The losses are estimated by measuring 1 cm long waveguides on several samples to be approximately 2 dB/cm, and the fiber chip coupling is around 9–10 dB, comparable with the results in [7].

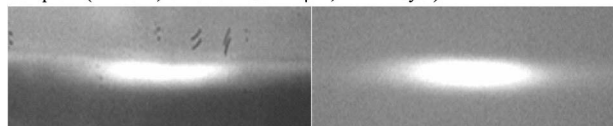
In conclusion, the DUV integrated reverse symmetry waveguide is a novel addition to the DUV Bio-Fluidic-Photonics technology platform [13] for realizing optical devices with a defined evanescent field area required in couplers or sensors. Moreover, defined patterning of the porous Si layer, as for example described in [14], in combination with our described fabrication process enables the realization of defined waveguide regions having a larger evanescent field than in other parts of the integrated waveguide device, which we intend to leverage in cell-based biosensor studies.

D. G. Rabus acknowledges support from the Alexander von Humboldt Foundation. L. A. DeLouise acknowledges support from the National Institutes of Health, grant NIAID 5 K25 AI00884.

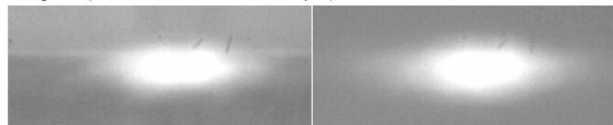
## References

1. R. C. Nesnidal and T. G. Walker, *Appl. Opt.* **35**, 2226 (1996).
2. G. R. Quigley, R. D. Harris, and J. S. Wilkinson, *Appl. Opt.* **38**, 6036 (1999).
3. D.-K. Qing and G. Chen, *Appl. Phys. Lett.* **84**, 669 (2004).
4. R. Horvath, L. R. Lindvold, and N. B. Larsen, *Appl. Phys. B: Lasers Opt.* **74**, 383 (2002).
5. R. Horvath and H. C. Pedersen, *Appl. Phys. Lett.* **81**, 2166 (2002).
6. L. A. DeLouise and B. L. Miller, *Proc. SPIE* **5357**, 111 (2004).
7. R. L. Oliveri, A. Sciuto, S. Libertino, G. D'Arrigo, and C. Arnone, in *Proceedings of 2005 IEEE/LEOS Workshop on Fibres and Optical Passive Components* (IEEE-LEOS, 2005), pp. 265–270.
8. P. Henzi, K. Bade, D. G. Rabus, and J. Mohr, *J. Vac. Sci. Technol. B* **24**, 1755 (2006).
9. D. G. Rabus, P. Henzi, and J. Mohr, *IEEE Photon. Technol. Lett.* **3**, 591 (2005).
10. Y. G. Zhao, W. K. Lu, Y. Ma, S. S. Kim, S. T. Ho, and T. J. Marks, *Appl. Phys. Lett.* **77**, 2961 (2000).
11. R. Horvath, H. C. Pedersen, N. Skivesen, C. Svanberg, and N. B. Larsen, *J. Micromech. Microeng.* **15**, 1260 (2005).
12. D. A. G. Bruggeman, *Ann. Phys. (Paris)* **24**, 636 (1935).
13. D. G. Rabus, M. Bruendel, Y. Ichihashi, A. Welle, R. A. Seger, and M. A. Isaacson, *IEEE J. Sel. Top. Quantum Electron.* **13**, 214 (2007).
14. J. D. L. Shapley and D. A. Barrow, *Thin Solid Films* **388**, 134 (2001).

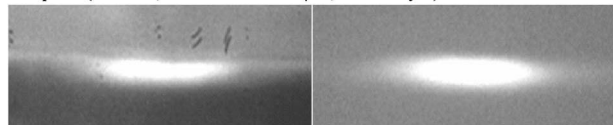
Sample 5 (RI=1.21; NP thickness = 8  $\mu\text{m}$ ; 12 nm layer)



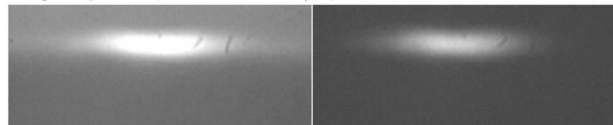
Sample 3 (RI=1.21; NP thickness = 4  $\mu\text{m}$ )



Sample 2 (RI=1.38; NP thickness = 4  $\mu\text{m}$ ; 12 nm layer)



Sample 4 (RI=1.21; NP thickness = 8  $\mu\text{m}$ )



Mode profile of bulk polymer DUV waveguide without water for comparison

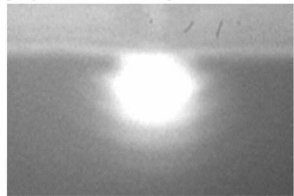


Fig. 3. Near-field analysis of integrated reverse symmetry waveguide samples: left, without water; right, with water. Sample 5, evanescent field enhancement observed, which is attributed to the 12 nm intermediate layer. Sample 3, evanescent field enhancement not observed, no barrier layer present. The field also decays more into the PSi layer when compared with sample 5. Sample 2, evanescent field enhancement observed despite the higher value of 1.38 for the index of the lower cladding. Sample 4, evanescent field enhancement not observed, no barrier layer present. The illumination and camera parameters are unchanged throughout the entire near-field measurements to guarantee compatibility of the images.